Adiabatic path integral molecular dynamics methods. II. Algorithms

J. Cao
Department of Chemistry, University of Pennsylvania, Philadelphia, Pennsylvania 19104-6323

G. J. Martyna
Department of Chemistry, Indiana University, Bloomington, Indiana 47405-4001

(Received 1 February 1995; accepted 9 October 1995)

Efficient numerical algorithms are developed for use with two finite temperature semiclassical approximations to quantum dynamics both of which require trajectories generated on potentials of mean force derived from the path integral expression for the density matrix. The numerical algorithms are formed from the combination of a classical adiabatic relation similar to that used in the Car–Parrinello method and an efficient path integral molecular dynamics scheme. Results on model, an anharmonic oscillator and a realistic, fluid *para*-hydrogen, problem indicate that semiclassical dynamics can be obtained for virtually the same computational cost as structure and thermodynamics. © *1996 American Institute of Physics.* [S0021-9606(96)50203-1]

I. INTRODUCTION

Despite the fact that the thermodynamic and structural properties of quantum many body systems can now, routinely be determined using path integral Monte Carlo or molecular dynamics methods,[1–4] it is not, yet, possible to efficiently calculate the corresponding quantum dynamical properties. It is, therefore, worthwhile to investigate semiclassical alternatives that can yield approximate quantum dynamics, at the same computational cost as structure and thermodynamics.

A semiclassical, finite temperature, quantum dynamics scheme based on the use of classical time correlation functions generated on the potential of mean force of the path integral centroid has been developed.[5–9] The method has been shown to give the exact quantum position and velocity autocorrelation functions of quadratic actions, contain the classical limit and when used as statistical theory give the correct rate constant for a parabolic barrier. A similar theory which utilizes the potential of mean force on a path integral bead has also been developed.[10] Numerical methods capable of generating these semiclassical dynamics schemes, without the exhaustive enumeration of the necessary potentials of mean force, are presented. The algorithms are based on the coupling of an efficient path integral molecular dynamics (PIMD) scheme[4] to a Car–Parrinello-like[11,12] classical adiabatic principle. Tests of the methods on model, an anharmonic oscillator and realistic problems, fluid *para*-hydrogen, indicate that semiclassical dynamics can be generated for virtually the same computational cost as thermodynamics and structure. Other useful numerical methods for centroid dynamics have been presented elsewhere.[5–8]

II. THEORY

In this section, two semiclassical quantum dynamics methods, path integral centroid dynamics and path integral Wigner dynamics are briefly described.

A. Centroid and Wigner dynamics

Centroid semiclassical dynamics[5–8] is based on the use of the path integral centroid density as a semiclassical phase space function

$$\begin{aligned} &W_c(v,x_c;\beta)=K\ \exp(-\beta[V^{(\mathrm{eff})}(x_c)+T^{(\mathrm{eff})}(v_c)]),\\ &\left[\frac{\beta m}{2\pi}\right]^{1/2}\exp\left[-\frac{\beta m v_c^2}{2}\right]=K\ \exp[-\beta T^{(\mathrm{eff})}(v_c)],\\ &N_{\rho_c}\rho(x_c;\beta)=\exp[-\beta V^{(\mathrm{eff})}(x_c)],\\ &\rho(x_c;\beta)=\int dx_1\ldots dx_P\prod_{i=1}^{P}\rho\left(x_i,x_{i+1};\frac{\beta}{P}\right)\\ &\qquad\times\delta\left(x_c-\frac{1}{P}\sum_{i=1}^{P}x_i\right), \end{aligned} \tag{2.1}$$

where $x_{P+1}=x_1$. Time correlation function calculated using centroid phase space function, can be related to the real part of the true quantum result, $\bar{C}_{xx}^{(\mathrm{quant})}$, by[5–8]

$$\tilde{\bar{C}}_{xx}^{(\mathrm{quant})}(\omega)\sim\left[\frac{(\beta\hbar\omega/2)}{\tanh(\beta\hbar\omega/2)}\right]\tilde{C}_{x_cx_c}^{(\mathrm{centroid})}(\omega), \tag{2.2}$$

where $\tilde{C}(\omega)$ signifies the Fourier transform of $C(t)$ as centroid MD generate an approximation to the Kubo transformed time correlation function. The expression is exact for quadratic potentials. Another relationship gives the imaginary part of the time correction function in terms of the Kubo-transformed variant.[8]

In analogy with the centroid method, path integral separable second moment Wigner semiclassical dynamics is based on the separable second moment Wigner semiclassical phase space density[10,13–16]

$$\begin{aligned} W_{ssw}(v,x;\beta)&=P_v(v;\beta)P_x(x;\beta)\\ &=K\ \exp[-\beta H^{(\mathrm{eff})}(v,x;\beta)],\\ P_x(x;\beta)&=N_\rho\rho(x,x;\beta)=\exp[-\beta V^{(\mathrm{eff})}(x;\beta)], \end{aligned} \tag{2.3}$$

 0021-9606/96/104(5)/2028/8/$10.00

$$P_v(v;\beta)=\frac{1}{N_\rho}\left[\frac{\beta m^{(\mathrm{eff})}(\beta)}{2\pi}\right]^{1/2}\exp\left[-\frac{\beta m^{(\mathrm{eff})}(\beta)v^2}{2}\right],$$

$$m^{(\mathrm{eff})}(\beta)=\frac{m}{2\beta T},$$

where $\bar{T}$ is the average kinetic energy. The semiclassical Hamiltonian, $H^{(\mathrm{eff})}(v,x;\beta)$, can be used to generate semiclassical correlation functions which are exact for quadratic problems. Note, in many body systems, the effective masses, $m^{(\mathrm{eff})}(\beta)$, must be introduced in an appropriate set of normal modes.[10] This is problematic in a quantum liquid where a fixed set of normal modes does not exist and the method will be shown to fail.

A higher order approximation, path integral nonseparable Wigner semiclassical dynamics is based on a nonseparable Wigner semiclassical phase space density[10]

$$W_{nW}(v,\bar{x};\beta)=K\,\exp\left(-\beta\left[\frac{m^{(\mathrm{eff})}(\bar{x};\beta)v^2}{2}+V^{(\mathrm{eff})}(\bar{x};\beta)\right]\right),$$

$$\exp[-\beta V^{(\mathrm{eff})}(x;\beta)]=N_\rho(x)\rho(x,x;\beta),$$

$$N_\rho(x)=\left[\frac{m^2}{2\pi\hbar^2\beta m^{(\mathrm{eff})}(x;\beta)}\right]^{-1/2}, \tag{2.4}$$

$$[m^{(\mathrm{eff})}(x,\beta)]^{-1}=\frac{2\beta}{m}\,T^{(\mathrm{loc})}(x;\beta),$$

$$T^{(\mathrm{loc})}(x;\beta)=-\frac{\hbar^2}{8m\rho(x,x;\beta)}\left[\frac{\partial^2\rho(x,x';\beta)}{\partial x^2}-2\frac{\partial^2\rho(x,x';\beta)}{\partial x\,\partial x'}+\frac{\partial^2\rho(x,x';\beta)}{\partial(x')^2}\right]\Bigg|_{\lim x=x'},$$

$$T^{(\mathrm{loc})}(x_1,\beta)=\frac{\int dx_2\cdots\int dx_P[\Pi_i\rho(x_i,x_{i+1};\beta/P)]T^{(\mathrm{est})}(X,\beta)}{\int dx_2\cdots\int dx_P[\Pi_i\rho(x_i,x_{i+1};\beta/P)]},$$

$$T^{(\mathrm{est})}(X;\beta)=\frac{1}{2\beta}+\frac{\hbar^2\beta}{\delta mP}\sum_{k=1}^{P}\left[1-\frac{2(k-1)}{P}\right]^2\frac{\partial^2 v(x_k)}{\partial x_k^2}-\frac{\hbar^2\beta^2}{8m}\left[\frac{i}{P}\sum_{k=2}^{P}\left[1-\frac{2(k-1)}{P}\right]^2\frac{\partial V(x_k)}{\partial x_k}\right]^2,$$

where $x_{P+1}=x_1$. It is more difficult to use than the separable second moment approximation because the associated equations of motion

$$\dot{x}=v\left(\frac{m^{(\mathrm{eff})}(x;\beta)}{\bar{m}^{(\mathrm{eff})}(\beta)}\right),$$

$$\dot{v}=\frac{F^{(\mathrm{eff})}(x;\beta)}{\bar{m}^{(\mathrm{eff})}(\beta)}-\left(\frac{m^{(\mathrm{eff})}(x;\beta)v^2}{2\bar{m}^{(\mathrm{eff})}(\beta)}\right)\frac{d\,\log[m^{(\mathrm{eff})}(x;\beta)]}{dx}, \tag{2.5}$$

where

$$\bar{m}^{(\mathrm{eff})}(\beta)=\left[\frac{m\langle m^{(\mathrm{eff})}(x,\beta)\rangle}{2\beta T}\right]^{1/2}, \tag{2.6}$$

do not lend themselves to a straightforward application of an adiabatic dynamics method (see below). In one dimension, it is straight forward to enumerate $m^{(\mathrm{eff})}(x;\beta)$, and apply an adiabatic dynamics method. However, in a realistic system such as a quantum liquid, the position dependent effective mass is a tensor that must be generated on the fly. Efficient numerical methods capable of handling this situation are currently being developed.

III. NUMERICAL METHODS

The different semiclassical dynamics methods described above, centroid and Wigner, require the motion of a variable on a true quantum mechanical potential of mean force. The adiabatic path integral centroid and path integral (separable) Wigner molecular dynamics methods (ACPIMD and ASWPIMD) capable for generating this dynamics are formed by the combination of an efficient path integral molecular dynamics method (PIMD)[4] and a classical adiabatic principle. The basic PIMD method, the adiabatic principle and their combination which defines ACPIMD and ASWPIMD are described below.

A. PIMD

In order to derive a path integral molecular dynamics algorithm, the discrete path integral expression for the canonical partition function, Q,[17–20] is written in the form of a *fictitious* phase space integral by introducing P momenta with arbitrary mass, m_c,[11,21] conjugate to the coordinates

$$Q=f(m,m_c,\beta,P)\int dx_1\ldots dx_P\int dp_1\ldots dp_P\times\exp\left(-\beta\sum_{i=1}^{P}\left[\frac{p_i^2}{2m_c}+\frac{mP}{2\hbar^2\beta^2}(x_i-x_{i+1})^2+\frac{1}{P}V(x_i)\right]\right), \tag{3.1}$$

where $f(m,m_c,\beta,P)$ represents the overall normalization. The effective classical Hamiltonian associated with this partition function,

$$H=\sum_{i=1}^{P}\left[\frac{p_i^2}{2m_c}+\frac{1}{2}m\omega_P^2(x_i-x_{i+1})^2+\frac{1}{P}V(x_i)\right],\qquad \omega_P\equiv\frac{\sqrt{P}}{\beta\hbar}, \tag{3.2}$$

can be used to define a molecular dynamics sampling tool.

Path integrals are notoriously difficult to evaluate using molecular dynamics (MD) methods.[1] The stiff harmonic terms or bonds present in the classical Hamiltonian, Eq. (3.2), give rise to a nonergodic dynamics, a MD time step that decreases as the square root of the number discretizations, $P^{1/2}$, and a slow sampling of the available phase space due to the wide range of normal mode frequencies (associated with the bonds). These problems can be overcome through the combination of several methods.[4,22–24] The massive Nosé–Hoover chain canonical dynamics method gives

an ergodic canonical dynamics, multiple time step integration eliminates the $P^{1/2}$ dependence of the time step and a noncanonical transformation of variables places the normal modes on the same frequency scale. The coupling of the massive Nosé–Hoover chain canonical dynamics method[4,22,23] (one Nosé–Hoover chain per degree of freedom) to multiple time integration[24] is discussed, in detail, elsewhere.[4] The appropriate variable changes are reviewed below.

There are two variables transformations of interest here. The first transformation, useful in centroid dynamics, is to the set of normal modes (P even)[25]

$$x_n=\sum_{k=1}^{P} a_k \exp\left[\frac{2\pi i(n-1)(k-1)}{P}\right], \tag{3.3}$$

where $a_1=\mathrm{Re}(a_1)$, $a_{(P+2)/2}=\mathrm{Re}(a_{(P+2)/2})$, $a_{P-k+2}=a_k^*$ and

$$\begin{aligned} &u_1=a_1; \quad u_P=a_{(P+2)/2}, \\ &u_{2k-2}=\mathrm{Re}(a_k); \quad u_{2k-1}=\mathrm{Im}(a_k) \end{aligned} \tag{3.4}$$

define the P independent variables.[5–8] The associated classical Hamiltonian is

$$\begin{aligned} &H=\sum_{i=1}^{P}\left[\frac{p_{u_i}^2}{2m_{u_i}}+\frac{1}{2}m\omega_P^2\lambda_i u_i^2+\frac{1}{P}V(x_i(\mathbf{u}))\right], \\ &\lambda_1=0; \quad \lambda_P=4P, \\ &\lambda_{2k-1}=\lambda_{2k-2}=4P\left[1-\cos\left(\frac{2\pi(k-1)}{P}\right)\right]. \end{aligned} \tag{3.5}$$

(This is only equivalent to Fourier path integrals in the $P=\infty$ limit.[26]) The transformation is noncanonical because the masses, the m_{u_i} are chosen to be $\{m_{u_1}=m, m_{u_k}=m\lambda_c^2\lambda_k\}$ so that all the modes have the same frequency. Fast Fourier transforms (FFTs) can be used to switch back and forth between the Cartesian and normal mode coordinates as well as to generate the forces on the normal modes from the forces on the Cartesian variables (see the Appendix). One is not necessarily restricted to $P=2^n$ as modern FFT packages will, in general, contain efficient $P=2^n3^m5^l$ radix methods.

The second transformation, useful in path integral separable second moment Wigner dynamics, is to the staging coordinates,[2,4]

$$u_1=x_1, \quad u_k=x_k-x_k^*, \quad x_k^*=\frac{(k-1)x_{k+1}+x_1}{k}. \tag{3.6}$$

The inverse transformation is

$$x_1=u_1, \quad x_k=u_k+\frac{k-1}{k}x_{k+1}+\frac{1}{k}x_1. \tag{3.7}$$

Here, the associated classical Hamiltonian is

$$\begin{aligned} &H=\sum_{i=1}^{P}\frac{p_{u_i}^2}{2m_{u_i}}+\sum_{k=2}^{P}\frac{1}{2}m_k\omega_P^2u_k^2+\frac{1}{P}\sum_{i=1}^{P}V(x_i(u)), \\ &m_k=m\left(\frac{k}{k-1}\right), \end{aligned} \tag{3.8}$$

where the masses, $\{m_{u_1}=m/(2\beta\bar{T}), m_{u_k}=\gamma_s^2m_k\}$, are again, chosen to give all the modes the same frequency. For simplicity u_1 will be referred to as "the" staging bead and the other u_k as the staging modes. More general staging transformations and the method of application (the analog of the Appendix) are presented elsewhere.[4] The forward and backward staging transformations are very fast because of their simple recursive nature. Note, the staging Hamiltonian is invariant to a cyclic relabeling of the Cartesian positions, $x_i\rightarrow x_{i+L}$ where $i+L=i+L-P$ if $i+l>P$, although the transform alters the specific values of the u's. This relabeling operation is referred to as a mass rotation.[4] A third transformation[27]

$$x_k=u_1+\left(\frac{2}{P}\right)^{1/2}\sum_{m=2}^{P}u_m\sin\left(\frac{(m-1)(k-1)\pi}{P}\right) \tag{3.9}$$

which can, also, be applied using FFTs is not as computational efficient as the staging method.

The transformations defined above give rise to the same expression for the force on the centroid coordinate as for the force on the staging bead,

$$F_1=\frac{1}{P}\sum_{i=1}^{P}\nabla_i V(x_i). \tag{3.10}$$

If the potential is quadratic then $F_1=-m\omega^2x_c$ where x_c is, in fact, the centroid coordinate.

B. Adiabatic dynamics

A general treatment of adiabatic dynamics has been presented elsewhere.[12] Some of the arguments have been repeated here for completeness. Consider two set of degrees of freedom, $\{\mathbf{v}_x,\mathbf{x}\}$ and $\{\mathbf{v}_y,\mathbf{y}\}$, undergoing Nosé–Hoover chain canonical dynamics

$$\begin{aligned} &\dot{\mathbf{x}}=\mathbf{v}_x, \quad \dot{\mathbf{y}}=\mathbf{v}_y, \quad \dot{\mathbf{v}}_x=\frac{\mathbf{F}_x(\mathbf{x},\mathbf{y})}{2m_x}-\mathbf{v}_x\upsilon_{\eta(x,1)}, \\ &\dot{\mathbf{v}}_y=\frac{\mathbf{F}_y(\mathbf{x},\mathbf{y})}{2m_y}-\mathbf{v}_y\upsilon_{\eta(y,1)}, \quad \dot{\eta}_\alpha=\upsilon_{\eta(\alpha,1)}, \\ &\dot{\upsilon}_{\eta(\alpha,1)}=\frac{1}{Q_{\eta(\alpha,1)}}\left[\sum_k m_\alpha\mathbf{v}_{\alpha_k}^2-N_\alpha kT_\alpha\right]-\upsilon_{\eta(\alpha,1)}\upsilon_{\eta(\alpha,2)}, \\ &\dot{\upsilon}_{\eta(\alpha,k)}=\frac{1}{Q_{\eta(\alpha,k)}}\left[Q_{\eta(\alpha,k-1)}\upsilon_{\eta(\alpha,k-1)}^2-kT_\alpha\right] \\ &\qquad -\upsilon_{\eta(\alpha,k)}\upsilon_{\eta(\alpha,k+1)}, \\ &\dot{\upsilon}_{\eta(\alpha,M)}=\frac{1}{Q_{\eta(\alpha,M)}}\left[Q_{\eta(\alpha,M-1)}\upsilon_{\eta(\alpha,M-1)}^2-kT_\alpha\right], \end{aligned} \tag{3.11}$$

where α is summed over both x and y and M is the number of thermostats ($\eta_{(\alpha)}$'s) in the two Nosé–Hoover chains. Note,

different temperatures, T_x/T_y, have been associated with the x/y degrees of freedom. The Liouville operator for this dynamics is

$$
\begin{aligned}
iL &= iL_x + iL_y + iL_x^{(\mathrm{NHC})} + iL_y^{(\mathrm{NHC})},\\
iL_x &= \mathbf{v}_x\cdot\boldsymbol{\nabla}_x + \frac{\mathbf{F}_x(\mathbf{x},\mathbf{y})}{2m_x}\cdot\boldsymbol{\nabla}_{v_x} - v_{\eta(x,1)}\mathbf{v}_x\cdot\boldsymbol{\nabla}_{v_x},\\
iL_y &= \mathbf{v}_y\cdot\boldsymbol{\nabla}_y + \frac{\mathbf{F}_y(\mathbf{x},\mathbf{y})}{2m_y}\cdot\boldsymbol{\nabla}_{v_y} - v_{\eta(y,1)}\mathbf{v}_y\cdot\boldsymbol{\nabla}_{v_y},\\
iL_\alpha^{(\mathrm{NHC})} &= \sum_{k=1}^{M} v_{\eta(\alpha,k)}\frac{d}{d\eta_{(\alpha,k)}}\\
&\quad + G(\mathbf{v}_\alpha,N_\alpha,T_\alpha,Q_{(\alpha,1)})\frac{d}{dv_{\eta(\alpha,1)}}\\
&\quad + \sum_{k=2}^{M} G(v_{\eta(\alpha,k-1)},1,T_\alpha,Q_{(\alpha,k)})\frac{d}{dv_{\eta(\alpha,k)}}\\
&\quad - \sum_{k=1}^{M-1} v_{\eta(\alpha,k)}v_{\eta(\alpha,k+1)}\frac{d}{dv_{\eta(\alpha,k)}},\\
G(\mathbf{v},N,T,Q) &= \frac{1}{Q}\left[\sum_{k=1}^{N} m_k\mathbf{v}_k\cdot\mathbf{v}_k - NkT\right].
\end{aligned}
\tag{3.12}
$$

In the limit that the **x** variables are moving fast compared to the **y** variables, the evolution operator for the dynamics can be written as

$$
\begin{aligned}
\exp[iL\Delta t] &= \exp\left[(iL - iL^{(\mathrm{ref})})\frac{\Delta t}{2}\right]\exp[iL^{(\mathrm{ref})}\Delta t]\\
&\quad\times\exp\left[(iL - iL^{(\mathrm{ref})})\frac{\Delta t}{2}\right],\\
iL^{(\mathrm{ref})} &= iL_y + iL_y^{(\mathrm{NHC})} - \frac{\mathbf{F}_y(\mathbf{x},\mathbf{y})}{2m_y}\cdot\boldsymbol{\nabla}_{v_y}.
\end{aligned}
$$

The solution to the equations of motion for the **y** subsystem determined from this approximate evolution operator is,

$$
\begin{aligned}
\mathbf{y}(\Delta t) &= \mathbf{y}^{(\mathrm{ref})}[\mathbf{y}(0),\mathbf{v}_y(\Delta t/2),\mathbf{v}_{\eta_y}(0);\Delta t],\\
\mathbf{v}_y(\Delta t) &= \mathbf{v}_y^{(\mathrm{ref})}[\mathbf{y}(0),\mathbf{v}_y(\Delta t/2),\mathbf{v}_{\eta_y}(0);\Delta t]\\
&\quad + \frac{1}{m_y}\int_0^{\Delta t/2} dt'\ \mathbf{F}_y\{\mathbf{x}^{(\mathrm{adb})}\\
&\quad\times[\mathbf{x}(\Delta t/2),\mathbf{v}_x(\Delta t/2),\mathbf{v}_{\eta_x}(\Delta t/2);t'],\mathbf{y}(\Delta t)\},
\end{aligned}
\tag{3.13}
$$

$$
\mathbf{v}_y(\Delta t/2) = \mathbf{v}_y(0) + \frac{1}{m_y}\int_0^{\Delta t/2} dt'\ \mathbf{F}_y\{\mathbf{x}^{(\mathrm{adb})}\times[\mathbf{x}(0),\mathbf{v}_x(0),\mathbf{v}_{\eta_x}(0);t'],\mathbf{y}(0)\}.
$$

The functions $\mathbf{x}^{(\mathrm{adb})}[\mathbf{x}',\mathbf{v}_x',\mathbf{v}_{\eta_x}';\mathbf{y}';t]$ and $\mathbf{v}_x^{(\mathrm{adb})}\times[\mathbf{x}',\mathbf{v}_x',\mathbf{v}_{\eta_x}';\mathbf{y};t]$ denote the positions and velocities at time, t, obtained from the Nosé–Hoover chain dynamics of the **x** subsystem with potential energy, $V(\mathbf{x},\mathbf{y})$, at fixed $\mathbf{y}'$ and initial condition, $\{\mathbf{x}',\mathbf{v}_x',\mathbf{v}_{\eta_x}'\}$. Similarly, the functions labeled, superscript (ref), refer to the action of the reference Liouville operator, $iL^{(\mathrm{ref})}$, on the **y** subsystem. If the time averages in the integrals are taken to the phase space averages than [i.e., the (adb) dynamics is ''ergodic'' on this time scale]

$$
\begin{aligned}
\mathbf{y}(\Delta t) &= \mathbf{y}^{(\mathrm{ref})}\Big[\mathbf{y}(0),\mathbf{v}_y(0)\\
&\quad + \frac{\Delta t}{2\beta_x m_y}\boldsymbol{\nabla}_y\log[Q_x(\beta_x,\mathbf{y}(0))],\mathbf{v}_{\eta_y}(0);\Delta t\Big],\\
\mathbf{v}_y(\Delta t) &= \mathbf{v}_y^{(\mathrm{ref})}\Big[\mathbf{y}(0),\mathbf{v}_y(0)\\
&\quad + \frac{\Delta t}{2\beta_x m_y}\boldsymbol{\nabla}_y\log[Q_x(\beta_x,\mathbf{y}(0))],\mathbf{v}_{\eta_y}(0);\Delta t\Big]\\
&\quad + \frac{\Delta t}{2\beta_x m_y}\boldsymbol{\nabla}_y\log[Q_x(\beta_x,\mathbf{y}(\Delta t))],
\end{aligned}
\tag{3.14}
$$

where $Q_x(\beta_x,y)$ is the canonical partition function of the **x** degrees of freedom at temperature, $kT_x = 1/\beta_x$ at fixed y. Furthermore, in the limit Δt goes to zero with the condition that the the mass of the **x** degrees of freedom is taken to zero fast enough that the time averages may be replaced by phase space averages, the evolution operator for reduced dynamics (i.e., the **y** subsystem) can be written as,

$$
\begin{aligned}
&\exp\left(\frac{\Delta t\overline{\mathbf{F}}(\mathbf{y})}{2m_y}\cdot\boldsymbol{\nabla}_{v_y}\right)\exp\left(\left[i\bar{L} - \frac{\overline{\mathbf{F}}(\mathbf{y})}{m_y}\cdot\boldsymbol{\nabla}_{v_y}\right]\Delta t\right)\\
&\quad\times\exp\left(\frac{\Delta t\overline{\mathbf{F}}(\mathbf{y})}{2m_y}\cdot\boldsymbol{\nabla}_{v_y}\right) = \exp(i\bar{L}\Delta t),
\end{aligned}
\tag{3.15}
$$

where

$$
\begin{aligned}
i\bar{L} &= \mathbf{v}_y\cdot\boldsymbol{\nabla}_y - v_{\eta_{(y,1)}}\mathbf{v}\cdot\boldsymbol{\nabla}_{v_y} + \frac{\overline{\mathbf{F}}(\mathbf{y})}{m_y}\boldsymbol{\nabla}_{v_y} + iL_{\mathrm{NHC}}^{y},\\
\overline{\mathbf{F}}(\mathbf{y}) &= -\boldsymbol{\nabla}_y\bar{V}(\mathbf{y};\beta_x),\\
\bar{V}(\mathbf{y};\beta_x) &= -\frac{1}{\beta_x}\log[Q_x(\beta_x,\mathbf{y})].
\end{aligned}
\tag{3.16}
$$

The analysis presented above demonstrates that under appropriate conditions, the slow subsystem, the **y**, at temperature, T_y, can be made to move on the potential of mean force generated by the fast subsystem, the **x**, at temperature, T_x (i.e., $\bar{V}(\mathbf{y};\beta_x)$). The traditional Car–Parrinello method[11] corresponds to T_x small so that $\bar{V}(\mathbf{y};\beta_x)$ is at a minimum with respect to the **x**. The methods of this paper require $T_y = T_x$. The third limit, $T_y \ll T_x$, the parametric minimization of the potential of mean force (i.e. $\bar{V}(\mathbf{y};\beta_x)$ is minimized with respect to **y**), is, also, of use in some applications.

C. Adiabatic centroid and Wigner PIMD

Centroid/separable Wigner semiclassical dynamics requires the centroid/staging degree of freedom to move on the

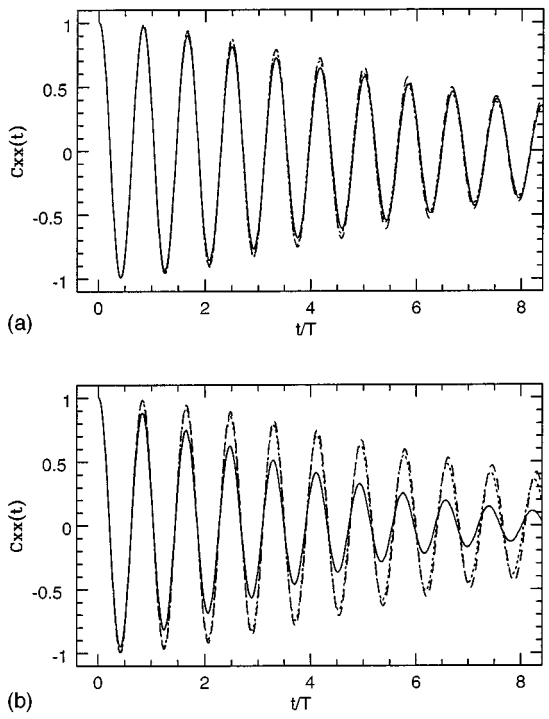

FIG. 1. (a) The real part of the position–position correlation function, $C_{xx}(t)$ for the model Hamiltonian, Eq. (4.1) calculated using ACPIMD. The time scale ratios, 1:1, the solid line, 4:1, the short dotted line, and 16:1, the long dashed lined are shown. (b) The real part of the position–position correlation function calculated using ASWPIMD. The time scale ratios, 1:1, the solid line, 4:1, the short dotted line, and 16:1, the long dashed lined are shown.

potential of mean force formed by the other modes in the problem. The coordinate systems defined in Sec. (III A), conveniently isolate the centroid/staging coordinates. It is, therefore, only necessary to adjust the parameter, γ_α, present in the masses of the normal/staging modes so that the massive Nosé–Hoover canonical dynamics of these subsidiary degrees of freedom is fast compared to the motion of desired the centroid/staging coordinate. No other programming or algorithmic changes are required.

It is not possible to straightforwardly apply an adiabatic dynamics method to generate, the nonseparable Wigner semiclassical dynamics because equations of motion

$$\ddot{x}=\frac{F^{(\mathrm{eff})}(x;\beta)m^{(\mathrm{eff})}(x;\beta)}{[\bar{m}^{(\mathrm{eff})}(\beta)]^2}+\frac{\dot{x}^2}{2}\frac{d\ \log[m^{(\mathrm{eff})}(x;\beta)]}{dx} \tag{3.17}$$

contain terms like $\langle F^{(\mathrm{eff})}(x;\beta)\rangle\langle m^{(\mathrm{eff})}(x;\beta)\rangle$. This situation requires the introduction of two independent path integral polymer chains and is quite a challenging numerical problem. However, in one dimensional systems, the effective mass can be independently enumerated and the adiabatic dynamics method directly applied (see Results section of Paper I).

IV. RESULTS

In this section, the semiclassical dynamics methods, adiabatic separable second momentum Wigner and adiabatic centroid path integral molecular dynamics (ASWPIMD and ACPIMD) are tested on both model and realistic problems.

A. Anharmonic oscillator

The ability of ASWPIMD and ACPIMD to efficiently produce the time correlation functions of the model Hamiltonian,[5–8]

$$\hat{H}=-\frac{\hbar^2}{2m}\frac{d^2}{dx^2}+\frac{m\omega^2x^2}{2}+gx^4, \tag{4.1}$$

where $m=1$, $\omega=1$, $g=0.1$, $m^{(\mathrm{eff})}=0.325$, at temperature, $\beta\hbar\omega=5$, is examined. The path integral was discretized into $P=128$ beads or imaginary time slices. In both methods, a time step of $0.08\gamma_\alpha/\omega$ where γ_α is the adiabaticity control parameter, was employed. Six hundred runs of length 16 harmonic periods were performed for each value of γ_α and used to generate the time correlation functions. In the centroid method, the velocity of the centroid coordinate (only) was resampled at the beginning of each run while in the Wigner method the velocity resampling of the staging bead

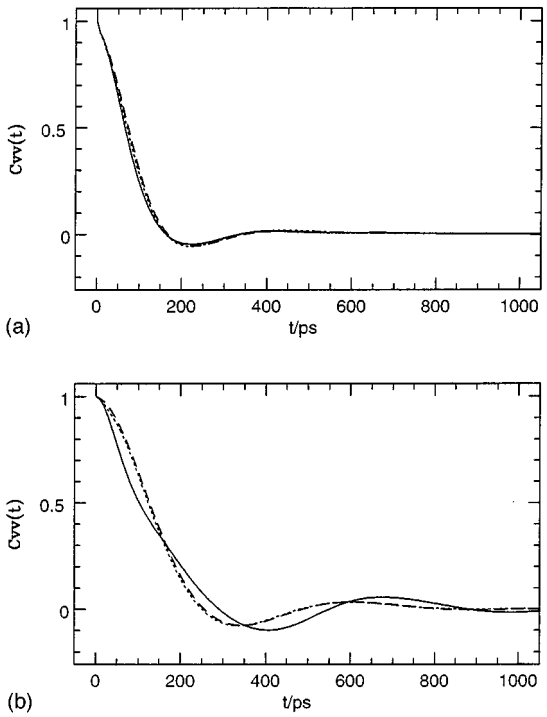

FIG. 2. (a) The velocity autocorrelation function of the molecular center of mass in fluid *para*-hydrogen at the state point, $\{T=25$ K, $V=31.7$ cm^3 mol$^{-1}\}$, calculated using ACPIMD. The time scale ratios, 1:1, the solid line, 4:1, the short dotted line and 16:1 the long dashed line are shown. (b) The velocity autocorrelation function of the molecular center of mass in fluid *para*-hydrogen at the state point, $\{T=25$ K, $V=31.7$ cm^3 mol$^{-1}\}$, calculated using ASWPIMD. The time scale ratios, 1:1, the solid line, 4:1, the short dotted line and 16:1 the long dashed line are shown.

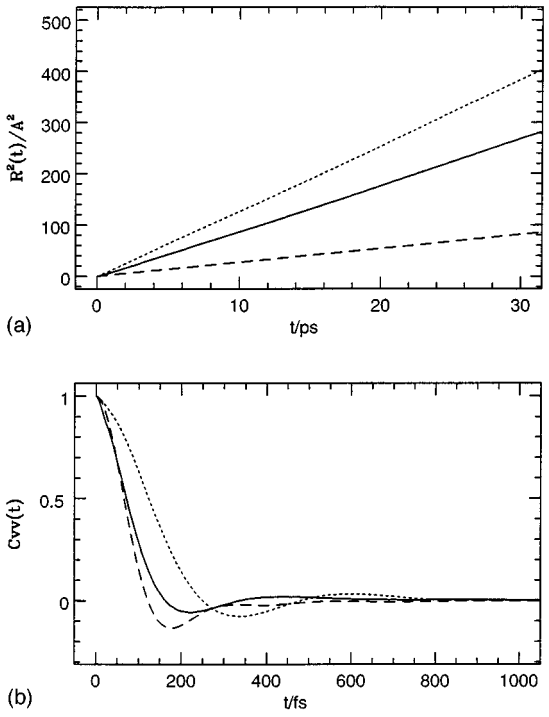

FIG. 3. (a) The Kubo transformed mean square displacement of the molecular center of mass in fluid *para*-hydrogen at the state point $\{T=25$ K, $V=31.7$ cm^3 mol$^{-1}\}$, calculated using centroid dynamics, the solid line, Wigner staging dynamics, the dotted line, and classical dynamics ($V=31.7$ cm^3 mol^{-1}), the long dashed line. (b) The velocity autocorrelation function of the molecular center of mass in fluid *para*-hydrogen at the state point $\{T=25$ K, $V=31.7$ cm^3 mol$^{-1}\}$, calculated using centroid dynamics, the solid line, Wigner staging dynamics, the dotted line and classical dynamics ($V=31.7$ cm^3 mol^{-1}), the long dashed line.

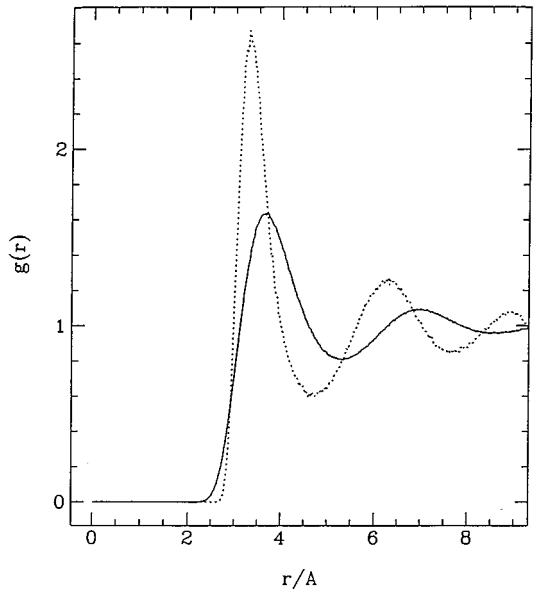

FIG. 4. The molecule center of mass pair distribution function for fluid *para*-hydrogen at $T=25$ K treated quantum mechanically ($V=31.7$ cm^3 mol^{-1}), the solid line, and treated classically ($V=20.2$ cm^3 mol^{-1}), the dotted line. In both the classical and quantum calculations, the average pressure is approximately zero.

coordinate was supplemented by a mass rotation (see Sec. III). Thermostats were coupled to each of the normal/staging modes but not to the centroid/staging bead.

The efficiency of the two numerical techniques, ASWPIMD and ACPIMD, is directly related to the ''separability'' of the forces in the two coordinate systems, staging and normal modes, respectively. In Sec. III, it was shown that the preaveraged expressions for the force on the staging bead and the centroid coordinate are the same, $F_{\rm pre}=(1/P)\Sigma_{i=1}^{P}F_i(x_i)$. For a harmonic oscillator, the centroid force is completely decoupled from the other centroid variables, $F_{\rm pre}=-\omega w x_c$, while the staging modes are strongly coupled. Therefore, ASWPIMD may require a larger adiabatic separation (smaller γ_α) than ACPIMD. In Fig. 4, the convergence of the two methods with increasing adiabatic separation (decreasing γ_α) is shown for the anharmonic oscillator. Unsurprisingly, the centroid method converges with almost no separation while the Wigner method requires a time dilation factor of at least 4. (An N:1 calculation requires a time of step of $0.08/(N\omega)$, i.e., $\gamma_\alpha=1/N$.) Thus ACPIMD is about a factor of 4 times more efficient then ASWPIMD for this simple example. Finally, the surprising similarity between the correlation functions produced by the two types methods, separable second moment Wigner dynamics and the centroid dynamics, should be noted. The exact correlation function has little decay on this time scale.[5,10] The nonseparable Wigner dynamics gives similar results (an enumerated position dependent effective mass is employed.)

B. Fluid *para*-hydrogen

The semiclassical dynamics methods, ACPIMD and ASWPIMD were tested on a realistic manybody problem, fluid *para*-hydrogen at the state point, $\{T=25$ K, $V=31.7$ cm^3 mol$^{-1}\}$ (approximately zero average pressure.[28,29] The *para*-hydrogen molecules were treated as spherical particles and a pair potential used to describe their interactions.[28–30] The minimum of the intermolecular *para*-hydrogen pair potential occurs at 3.44 Å and the well depth is 36 K. The mass of the particles are $m=3672$ a.u. The system size studied was $\{N=180, P=16\}$ where N is the number of particles and P is the number of discretizations of the path integral. The effective mass used in the separable second moment Wigner dynamics calculation was $m^{(\rm eff)}=2250$ a.u. A time steps of $7.5\gamma_\alpha$ fs was employed in all calculations. All runs were of length 75 ps. It should be noted that the ASWPIMD method can be expected to fail here as a straightforward scaling of the frequencies of all the modes is clearly too naive. The application of the higher level nonseparable Wigner dynamics to this problem is quite challenging and beyond the scope of this paper.

First, the convergence of the two methods, ACPIMD and ASWPIMD, with the degree of adiabatic separation is shown (Fig. 1). In Fig. 2, the Kubo transformed mean square displacement of the molecular center of mass are plotted for various separations in time scale (γ_α). Centroid dynamics converges with little or no adiabatic separation. Wigner dy-

TABLE I. Energetics of *para*-hydrogen, $P_{ext}\sim 0$. Qcal is the quantum path integral calculated value, Exp is the experimental value, Ccal is the corresponding value from the classical mechanics calculation, T is the temperature, $\langle E\rangle$ is the total energy, $\langle V\rangle$ is the potential energy, $\langle$KE$\rangle$ is the kinetic energy and $\langle$Vol$\rangle$ is the molar volume.

Label	T (K)	$\langle E\rangle$ (K)	$\langle V\rangle$ (K)	$\langle$KE$\rangle$ (K)	$\langle$Vol$\rangle$ (cm^3 mol^{-1})
Qcal	25	−47	−109	62	31.7
Ccal	25	−150	−187	38	20.2
Exp	25	−50			31.2
Qcal	14	−73	−135	62	25.6
Ccal	14	−222	−243	21	16.6
Exp	14	−75			26.2

namics requires a time dilation factor of approximately 4.

Next, the results of centroid dynamics and separable second moment Wigner dynamics are compared both to each other and classical mechanics. In Fig. 3, the Kubo transformed mean square displacement of the molecular center of mass and the molecular center of mass velocity autocorrelation function, calculated using the centroid method, the separable second moment Wigner method, as well as simple classical dynamics are presented. In the classical calculations, a molar volume of, $V^{(\mathrm{class})}=20.2$ cm^3 mol^{-1}, was used so that the average pressure of the classical system is approximately zero.[28] The quantum and classical molecular center of mass pair distribution functions (structure) are compared in Fig. 4 and the thermodynamic data is presented in Table I.[28,29]

The classical structure, dynamics and thermodynamics of *para*-hydrogen are completely different from their corresponding quantum mechanical counterparts (see Figs. 3 and 4 and in Table I). For example, the first peaks in the radial distribution and the zero pressure molar volumes differ by factors of 1.5 and diffusion coefficients by a factor of 3.[28,29] The classical and quantum velocity autocorrelation functions are also different. Unsurprisingly, classical mechanics is unable to describe the properties of fluid *para*-hydrogen.

The centroid and separable second moment Wigner method, also, give different results for the dynamical properties examined here. The centroid seems to be in good agreement with experiment, $D=1.6$ Å^2 ps^{-1} [31] while the separable second moment Wigner method is off by approximately 40%. Additional calculations at $\{T=14$ K, $V=25.6$ cm^3 mol$^{-1}\}$ (again, approximately zero average pressure[28,29]) show that the centroid method is in agreement with experiment while the Wigner based method has incurred about 40% error. At 14 K, the classical system is a solid. As stated above, the separable second moment Wigner method is likely in error because simply scaling frequencies by a constant factor is a rather poor approximation. Application of the higher level nonseparable Wigner semiclassical dynamics to this system awaits further methodological development.

TABLE II. Diffusion Coefficients of *para*-hydrogen, $P_{ext}\sim 0$. Qcal$_W$ is the value obtained from Wigner dynamics, Qcal$_C$ is the value obtained from centroid dynamics, Exp is the experimental value, Ccal is the corresponding classical value.

Label	T (K)	D (Å^2/ps)
Qcal$_W$	25	2.2
Qcal$_C$	25	1.5
Ccal	25	0.5
Exp	25	1.6
Qcal$_W$	14	0.55
Qcal$_C$	14	0.35
Ccal	14	
Exp	14	0.4

V. CONCLUSIONS

Numerical algorithms are developed for use with centroid dynamics and the separable second moment Wigner dynamics. The algorithms were found to be stable and efficient on both model and realistic problems. The centroid method, in particular, seems to give good results with little or no overhead. The overhead of the Wigner based method is approximately a factor of four. The two methods give remarkably similar results for the one dimensional model problem but behave differently in the nontrivial calculation of the properties of fluid *para*-hydrogen as expected. The centroid method seems to be give good agreement with experiment. Therefore, the structure and to a reasonable approximation to dynamics can be efficiently obtained in quantum mechanical manybody systems within the centroid framework. It will be of interest to see if the nonseparable Wigner theory is capable of correcting the results of the more basic second moment variant.

ACKNOWLEDGMENTS

This work was supported by startup funds provided by Indiana University and a grant from the Petroleum Research Fund (ACS-PRF 28968-G6). The authors would like to thank Professor Gregory Voth for comments on this work.

APPENDIX

Here, is the series of logical steps necessary to implement the centroid PIMD algorithm.

To get the forces on the normal modes:

(1) Set the real part of a complex vector equal to the Cartesian force $(I=1, P)$.
(2) Set the imaginary part of the complex vector equal to zero $(I=1, P)$.
(3) Perform an unscaled backward fast Fourier transform on the vector.
(4) The force on the (1)st mode is the real part of the 1st element of the transformed vector.
(5) The force on the (P)th mode is the real part of the $(P/2+1)$th element of the transformed vector.
(6) The force on the (1)st mode (the centroid) is the real part of the 1st element of the transformed vector.
(7) The force on the $(2I-2)$th mode is twice the real part of the Ith element of the transformed vector $(I=2, P/2)$.

(8) The force on the $(2I-1)$th mode is twice the imaginary part of the Ith element of the transformed vector $(I=2, P/2)$.

To transform the normal modes coordinates to Cartesian positions:

(1) Set the real part of the (1)st element of complex vector equal to the value of the (1)st mode (the centroid position).
(2) Set the real part of the $(P/2+1)$st element of the complex vector equal to the value of the Pth mode.
(3) Set the real part of the (I)th and the $(P-I+2)$th elements of the complex vector equal to the value of the $(2I-2)$th mode $(I=1, P/2)$.
(4) Set the imaginary part of the (I)th and the $(P-I+2)$th elements of the complex vector equal to the plus and minus the value of the $(2I-1)$th mode $(I=1, P/2)$, respectively.
(5) Perform an unscaled forward fast Fourier transform on the vector.
(6) The Cartesian position of the (I)th bead is equal to the real part of the Ith element of the transformed vector $(I=1, P)$.

To transform the Cartesian positions to normal modes coordinates:

(1) Set the real part of the Ith element of the a complex vector equal to the Cartesian position of the (I)th bead $(I=1, P)$.
(2) Perform a scaled backward fast Fourier transform on the vector.
(3) Set the value of the (1)st mode (the centroid position) equal to the real part of the (1)st element of the transformed vector.
(4) Set the value of the Pth mode equal to the real part of the $(P/2+1)$st element of the transformed vector.
(5) Set the value of the $(2I-2)$th mode equal to the real part of the (I)th element of the transformed vector $(I=2, P/2)$.
(6) Set the value of the $(2I-1)$th mode equal to the imaginary part of the (I)th element of the transformed vector $(I=2, P/2)$.

Free particle eigenvalue values of each normal modes:

(1) The eigenvalue of the (1)st mode is zero.
(2) The eigenvalue of the (P)th mode is $4P$.
(3) The eigenvalues of the $(2I-2)$th and the $(2I-1)$th modes are $4P[1-\cos(2\pi[I-1]/P)]$.

[1] B. J. Berne and D. Thirumalai, Ann. Rev. Phys. **37**, 401 (1986).
[2] E. L. Pollock and D. M. Ceperley, Phys. Rev. B **30**, 2555 (1984).
[3] J. D. Doll, T. F. Beck, and D. L. Freeman, J. Chem. Phys. **89**, 5753 (1988).
[4] M. E. Tuckerman, B. J. Berne, G. J. Martyna, and M. L. Klein, J. Chem. Phys. **99**, 2796 (1993).
[5] J. Cao and G. Voth, J. Chem. Phys. **99**, 10070 (1993).
[6] J. Cao and G. Voth, J. Chem. Phys. 100 (1994).
[7] J. Cao and G. Voth, J. Chem. Phys. (to be published).
[8] J. Cao and G. Voth, J. Chem. Phys. (to be published)
[9] G. Voth, D. Chandler, and W. H. Miller, J. Chem. Phys. **91**, 7749 (1989).
[10] G. J. Martyna, J. Chem Phys. **104**, 2018 (1996).
[11] R. Car and M. Parrinello, Phys. Rev. Lett. **55**, 2471 (1985).
[12] G. J. Martyna and M. L. Klein, J. Mol. Phys. (submitted).
[13] E. J. Heller, J. Chem. Phys. **65**, 1289 (1976).
[14] E. J. Heller, J. Chem. Phys. **67**, 3339 (1977).
[15] M. J. Davis and E. J. Heller, J. Chem. Phys. **80**, 5036 (1984).
[16] W. H. Miller, J. Chem. Phys. **61**, 1823 (1974).
[17] R. P. Feynman, *Statistical Mechanics* (Benjamin, Reading, 1972).
[18] L. D. Fosdick and H. F. Jordan, Phys. Rev. **143**, 58 (1966).
[19] J. A. Barker, J. Chem. Phys. **70**, 2914 (1978).
[20] M. Herman, E. F. Bruskin, and B. J. Berne, J. Chem. Phys. **76**, 1347 (1982).
[21] R. W. Hall and B. J. Berne, J. Chem. Phys. **81**, 3641 (1984).
[22] G. J. Martyna, M. E. Tuckerman, and M. L. Klein, J. Chem. Phys. **97**, 2635 (1992).
[23] D. J. Tobias, G. J. Martyna, and M. L. Klein, J. Phys. Chem. **97**, 12959 (1993).
[24] M. Tuckerman, G. J. Martyna, and B. J. Berne, J. Chem. Phys. **97**, 1990 (1992).
[25] J. Cao and B. J. Berne, J. Chem. Phys. **99**, 2902 (1993).
[26] R. D. Coalson, J. Chem. Phys. **85**, 926 (1986).
[27] J. Cao and B. J. Berne, J. Chem. Phys. **91**, 6359 (1989).
[28] D. Scharf, G. Martyna, and M. L. Klein, Low Temp. Phys. **19**, 365 (1993).
[29] D. Scharf, G. Martyna, and M. L. Klein, J. Chem. Phys. **99**, 8997 (1993).
[30] I. F. Silvera and V. V. Goldman, J. Chem. Phys. **69**, 4209 (1978).
[31] B. N. Esel'son, Yu. P. Blagoi, V. V. Grigor'ev, V. G. Manzhelii, S. A. Mikhailenko, and N. P. Neklyudov, *Properties of Liquid and Solid Hydrogen* (Israel Program for Scientific Translations, Jerusalem, 1971). Translated from Russian by Ch. Niesenbaum.